The habenular G-protein–coupled receptor 151 regulates synaptic plasticity and nicotine intake

Beatriz Antolin-Fontes[a], Kun Li[a], Jessica L. Ables[a,b,c], Michael H. Riad[a], Andreas Görlich[a], Maya Williams[b], Cuidong Wang[a], Sylvia M. Lipford[a], Maria Dao[b], Jianxi Liu[d], Henrik Molina[e], Nathaniel Heintz[a,1], Paul J. Kenny[b,d], and Ines Ibañez-Tallon[a1]

[a]Laboratory of Molecular Biology, The Rockefeller University, New York, NY 10065; [b]Nash Family Department of Neuroscience, Icahn School of Medicine at Mount Sinai, New York, NY 10029-6574; [c]Department of Psychiatry, Icahn School of Medicine at Mount Sinai, New York, NY 10029-6574; [d]Department of Pharmacology and Systems Therapeutics, Icahn School of Medicine at Mount Sinai, New York, NY 10029-6574; and [e]Proteomics Resource Center, The Rockefeller University, New York, NY 10065

Contributed by Nathaniel Heintz, January 17, 2020 (sent for review September 22, 2019; reviewed by Ana Belén Elgoyhen and Gord Fishell)

The habenula, an ancient small brain area in the epithalamus, densely expresses nicotinic acetylcholine receptors and is critical for nicotine intake and aversion. As such, identification of strategies to manipulate habenular activity may yield approaches to treat nicotine addiction. Here we show that GPR151, an orphan G-protein–coupled receptor (GPCR) highly enriched in the habenula of humans and rodents, is expressed at presynaptic membranes and synaptic vesicles and associates with synaptic components controlling vesicle release and ion transport. Deletion of *Gpr151* inhibits evoked neurotransmission but enhances spontaneous miniature synaptic currents and eliminates short-term plasticity induced by nicotine. We find that GPR151 couples to the G-alpha inhibitory protein $G\alpha_{o1}$ to reduce cyclic adenosine monophosphate (cAMP) levels in mice and in GPR151-expressing cell lines that are amenable to ligand screens. *Gpr151*– knockout (KO) mice show diminished behavioral responses to nicotine and self-administer greater quantities of the drug, phenotypes rescued by viral reexpression of *Gpr151* in the habenula. These data identify GPR151 as a critical modulator of habenular function that controls nicotine addiction vulnerability.

GPCR | IPN | spontaneous release | cAMP | self-administration

The global impact of nicotine addiction on health and economy is well documented (1). Currently, about one-third of the world's adult population smokes tobacco, and there is an alarming increase in the use of e-cigarettes (2). The tobacco epidemic kills nearly 7 million people a year, mainly from oral, esophageal, and lung cancers and cardiovascular diseases (1). Addiction is a chronic relapsing disorder characterized by compulsive drug seeking, escalation of intake, and development of affective and physical symptoms of withdrawal upon abrupt discontinuation or decrease in intake (3). Most drugs of abuse, including nicotine, as well as other reinforcing natural behaviors act on the mesocorticolimbic dopamine reward system (4, 5). However, stress and aversive stimuli activate and remodel partially overlapping networks within this system. For instance, other structures such as the habenula have been implicated in reward and aversion (6, 7). Increasing evidence suggests that the degree of sensitivity to both the rewarding and aversive aspects of an addictive drug and the severity of the withdrawal after discontinuing its use contribute to the addiction process (3). Understanding the mechanisms of these processes may reveal insights into the mechanics of the disorder and identify targets for medications development.

The habenula is a conserved diencephalic structure in the dorsal thalamus divided into medial (MHb) and lateral (LHb) domains (6, 8). The LHb receives and sends inputs to midbrain and hindbrain sites, while the MHb almost exclusively projects to the interpeduncular nucleus (IPN) via the fasciculus retroflexus (FR) (6, 8). MHb neurons are glutamatergic but use different neurotransmitter combinations (9); the superior part is glutamatergic, while the dorsal part of the central MHb coreleases substance P and glutamate, and the inferior, central, and lateral domains corelease acetylcholine and glutamate, which activate postsynaptic receptors via volume and wired transmission, respectively (10, 11). Some of the highest densities of nicotinic acetylcholine receptors (nAChRs) in the brain are detected in the MHb–IPN axis (12–15), especially of α5, α3, and β4 nAChR subunits. Little was known about the MHb in regulating the motivational properties of nicotine until human genetics studies established a strong association between genetic variants in the CHRNB4–A3–A5 gene cluster and smoking dependence (16), indicating that these nAChR subtypes are critical for acquisition of nicotine dependence and difficulties in smoking cessation. This prompted considerable interest in the role of MHb in nicotine addiction and led to investigations showing that the MHb exerts a key role in nicotine intake, aversion, withdrawal, and relapse (13, 17–19). Furthermore, it has been shown that chronic exposure to D-amphetamine, methamphetamine, MDMA, cocaine, or nicotine can induce degeneration of the FR, the main output tract of the habenula (6, 7). The finding that this descending pathway is compromised following drug binges has implications not only for theories of drug addiction but also for psychosis in general. Thus, the emerging picture is that the MHb–IPN pathway acts as an

Significance

Nicotine addiction affects one-third of the population and is the leading cause of preventable death. The habenula, an evolutionarily conserved brain structure, is enriched in nicotinic acetylcholine receptors (nAChRs) and critically controls nicotine intake. We found that GPR151, an orphan GPCR with selective expression in rodent and human habenular neurons, specifically regulates cyclic adenosine monophosphate levels and synaptic neurotransmission. Loss of GPR151 results in alterations of behaviors associated with nicotine and increases nicotine self-administration. Our study establishes that GPR151 regulates sensitivity and aversion to nicotine and suggests that small-molecule modulators of GPR151 may be useful for treatment of nicotine addiction.

Author contributions: N.H., P.J.K., and I.I.-T. designed research; B.A.-F., K.L., J.L.A., M.H.R., A.G., M.W., C.W., S.M.L., M.D., J.L., and H.M. performed research; B.A.-F., K.L., J.L.A., M.H.R., J.L., H.M., P.J.K., and I.I.-T. analyzed data; and B.A.-F., N.H., P.J.K., and I.I.-T. wrote the paper.

Reviewers: A.B.E., Instituto de Investigaciones en Ingenieria Genetica y Biologia Molecular (INGEBI-CONICET); and G.F., New York University Grossman School of Medicine, Harvard Medical School, and Broad Institute.

The authors declare no competing interest.

Data deposition: RNA sequencing data related to this paper have been deposited in the Gene Expression Omnibus (accession no. GSE143854).

[1]To whom correspondence may be addressed. Email: heintz@rockefeller.edu or iibanez@rockefeller.edu.

This article contains supporting information online at https://www.pnas.org/lookup/suppl/doi:10.1073/pnas.1916132117/-/DCSupplemental.

First published February 25, 2020.

inhibitory motivational signal that limits drug intake (17) and that alterations in the functioning of this pathway by drug consumption may contribute to aspects of addiction. Therefore, identification of a receptor that can regulate habenular neurons would be an ideal candidate for development of addiction therapies. Here we investigated the role of GPR151, an orphan G-protein–coupled receptor (GPCR) with selective expression in habenular axonal projections in regulating nicotine consumption.

Results

GPR151 Is Expressed at Axonal and Presynaptic Membranes and Synaptic Vesicles in Human and Rodent Habenula. GPR151 expression is conserved in the habenula of zebrafish, mice, and rats (20). Most *Gpr151*-expressing cells are concentrated in the MHb and a few scattered cells in the LHb (20, 21), as shown by in situ hybridization and translating ribosome affinity purification (TRAP) analysis (Fig. 1 *A* and *B* and *SI Appendix*, Figs. S1 and S2 *A* and *B*). GPR151 immunostaining is not detected in habenular cell bodies, but along their axonal projections that form the FR and terminate in the IPN (Fig. 1 *C* and *D*). Similarly, immunohistochemical localization of GPR151 in human brain shows that GPR151 specifically labeled axonal projections from MHb and LHb in the FR and IPN (Fig. 1 *E*–*K*). Western blot analyses show specific expression of GPR151 in human IPN samples (Fig. 1*L*). GPR151 is expressed mostly in MHb cholinergic neurons (70% of ChAT+ neurons express GPR151, Fig. 1*M* and *SI Appendix*, Fig. S2) highly enriched in nAChRs (Fig. 1*N* and *SI Appendix*, Fig. S2 *C*–*E*), but also in habenular neurons that are noncholinergic (30% approximately, *SI Appendix*, Fig. S2*B*). Since all neurons that originate in the MHb are glutamatergic (9, 10) we used the vesicular glutamate transporter 1 VGLUT1 to identify SVs corresponding to habenular axonal terminals and distinguish them from GABAergic postsynaptic neurons in the IPN. We performed immunoelectron microscopy (iEM) analyses in the rostral part of IPN (IPR, *SI Appendix*, Fig. S3*A*), which is most intensely labeled by GPR151 (20) and contains the highest concentration of cholinergic/glutamatergic axonal terminals (10). GPR151 immunoreactivity was observed in wild-type (WT) mice but not in *Gpr151*–knockout (KO) mice (*SI*

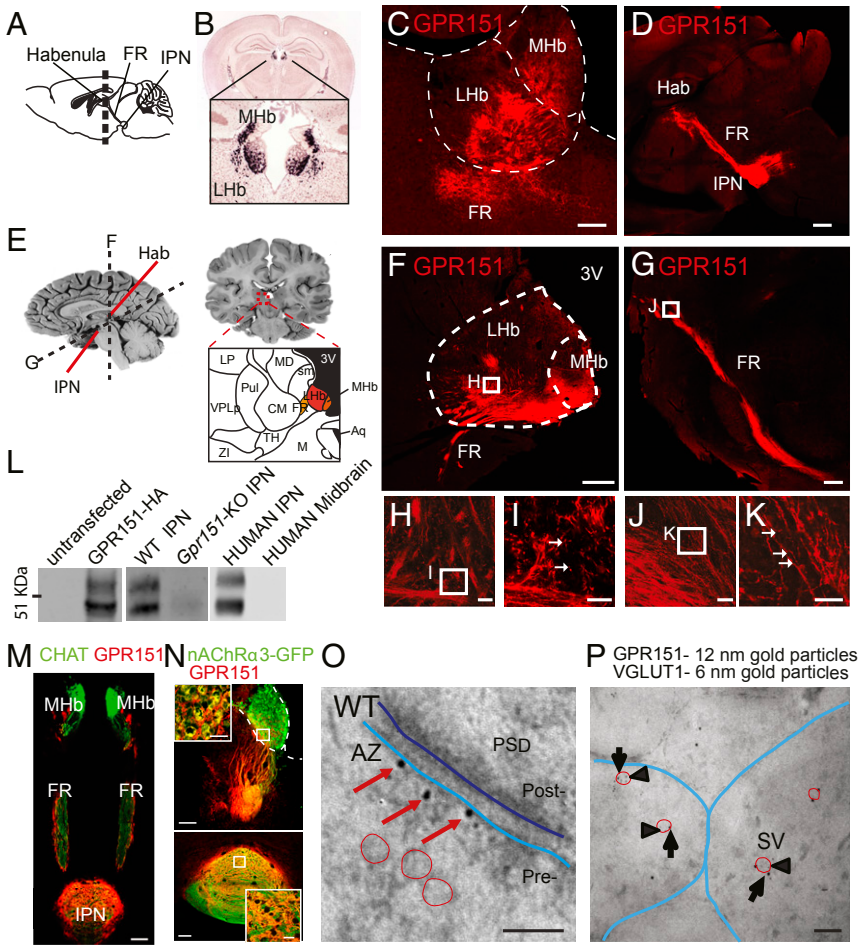

Fig. 1. GPR151 is enriched in the habenula of humans and rodents. (*A*) Mouse brain scheme indicating habenula (Hb), fasciculus retroflexus (FR), and interpeduncular nucleus (IPN). Dashed line indicates the plane of the coronal section shown in *B*. (*B*) In situ hybridization (46) shows *Gpr151* mRNA in cell bodies of MHb and LHb. (*C* and *D*) GPR151 immunohistochemistry in axonal fibers in Hb, FR, and IPN. (Scale bar, 100 μm in *C* and 500 μm in *D*.) (*E*) Schemes indicating the MHb, LHb, FR, and IPN in human brain. (*F*–*K*) GPR151 immunostaining in MHb, LHb, and FR of human brain samples. High-magnification pictures below. Arrows indicate GPR151 puncta along axons. (Scale bar, 1 mm in *F*, 500 μm in *G*, 50 μm in *H* and *J*, and 20 μm in *I* and *K*.) (*L*) Western blot of untransfected and GPR151–HA transfected HEK293 cells; IPN samples from WT, *Gpr151*–KO mice, human IPN, and human midbrain. Two bands (46 and 53 kDa) correspond to GPR151. (*M*) GPR151 immunohistochemistry in *Chat–ChR2* mice shows ChR2–EYFP (green) and GPR151 (red) in MHb cholinergic neurons. (Scale bar, 100 μm.) (*N*) GPR151 immunohistochemistry in *TgChrna3–EGFP* mice shows EGFP in MHb neurons expressing α3nAChRs (green) and GPR151 (red) in axons terminating in the IPN. (Scale bar, 100 μm.) (*O*) Electron microscopy (EM) micrographs of GPR151 immunogold particles (red arrows) at the presynaptic membrane (Pre; light blue line) of the active zone (AZ). Postsynaptic membrane (dark blue line), postsynaptic density (PSD), and synaptic vesicles (SVs; red circles) are indicated. (Scale bar, 100 nm.) (*P*) Double postembedding EM shows immunogold particles of GPR151 (12 nm, arrows) and VGLUT1 (6 nm, arrowheads) at SVs (red circles) close to presynaptic membranes (blue lines). (Scale bar, 100 nm.)

Appendix, Fig. S3 *B–G*), confirming the specificity of the antibody. GPR151 nanogold particles were located at the presynaptic plasma membrane (*SI Appendix*, Fig. S3 *B*, *C*, and *J*), at the active zone (AZ) (Fig. 1*O*) and in association with SVs (Fig. 1*P* and *SI Appendix*, Fig. S3 *H* and *J*) and dense core vesicles (*SI Appendix*, Fig. S3 *I* and *J*). GPR151 nanogold particles were also found along habenular axonal projections, mostly at the membrane but also along microtubules (*SI Appendix*, Fig. S3 *L* and *M*). This is interesting in light of recent findings showing that nAChRs are also expressed along Hb axons in the FR, where they can be activated by nicotine (22). Double postembedding iEM with VGLUT1 confirmed that GPR151 is at SVs (Fig. 1*P* and *SI Appendix*, Fig. S4 *A–F*) and transported along microtubules in axons (*SI Appendix*, Fig. S4 *G* and *H*). No significant differences in the synaptic terminal area, length of the AZ, diameter and density of SVs, and distance of SVs to the AZ were detected between WT and *Gpr151*–KO (*SI Appendix*, Fig. S4 *I–M*). The fact that *Gpr151*–KO mice have presynaptic terminals with normal morphology and SVs distribution argues against a role for GPR151 in synaptic scaffolding, cytoskeleton organization, or brain development. Rather, GPR151 localization at the synaptic and perisynaptic membrane and SVs suggests that GPR151 may modulate synaptic activity.

GPR151 Associates with Synaptic Components, Couples to the G-Alpha Inhibitory Protein Gαo1, and Regulates Cyclic Adenosine Monophosphate (cAMP) Levels. To understand the signaling mechanisms through which GPR151 controls habenular neurons we sought to identify its interacting partners, including which G-alpha protein subunit class (Gαs, Gαi, Gαq/11, or Gα12/13) it uses for signal transduction. We collected brain samples from IPNs of WT and *Gpr151*–KO mice, immunoprecipitated (IP) the protein extracts with GPR151 antibodies, and performed mass spectrometry analyses of IP samples (Fig. 2*A* and Dataset S1). As shown at the top right of the volcano plot (Fig. 2*B*), GPR151 is the most enriched protein in the immunoprecipitated fraction in WT mice, and it is not present in *Gpr151*–KO extracts, confirming the efficacy and specificity of the IPs. In addition, we identified 17 proteins that coimmunoprecipitated with GPR151 (Fig. 2*B*). These include SV proteins such

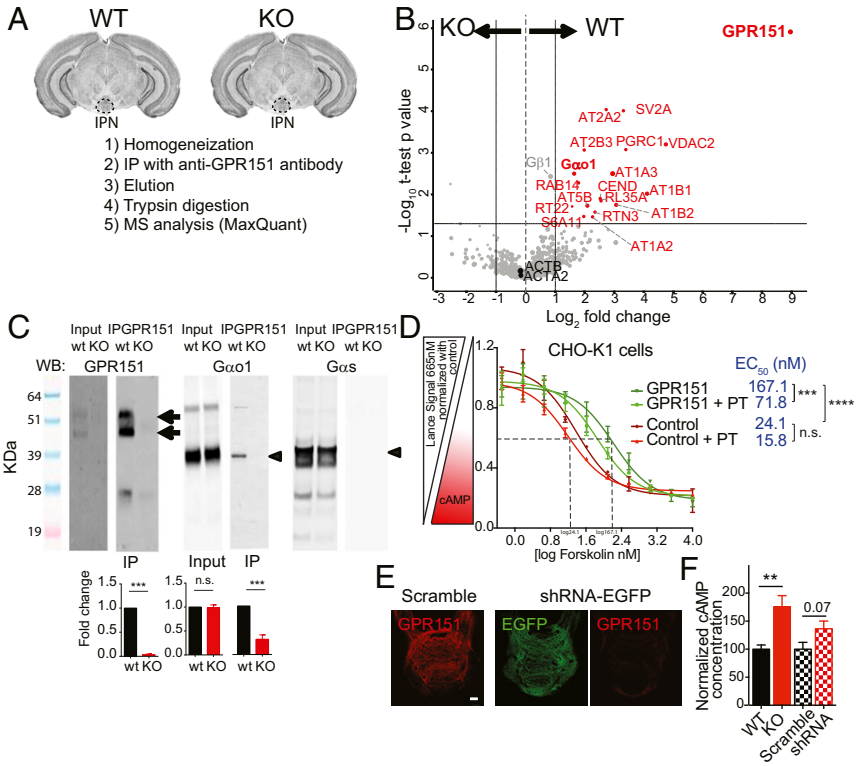

Fig. 2. GPR151 couples to the G-alpha inhibitory subunit $G\alpha_{o1}$ and coimmunoprecipitates with presynaptic regulators. (*A*) Outline of coimmunoprecipitation (co-IP) and Mass Spectrometry (MS) experiments ($n = 5$ biological replicates for WT and KO; 15 IPN per replicate).(*B*) Volcano plot of GPR151 co-IPed proteins from WT (*Right*) and *Gpr151*–KO (*Left*) IPN samples. Log2 ratios are plotted against the adjusted negative log10 *P* values. Significantly enriched co-IPed proteins ($P < 0.05$, Student *t* test) found in WT samples are labeled in red and include GPR151, $G\alpha_{o1}$, ATPases, and SV2A. Control proteins not enriched in WT (log2 < 1) include $G\beta_1$, ACTB1, and ACTA2, indicated in gray. (*C*) Western blot (WB) and quantification of GPR151, Gαo1, and Gαs in input (total lysate of WT and KO mice IPN samples) and immunoprecipitated (IP_{GPR151}) IPN brain samples. GPR151 IPs with Gαo1 (*Middle*) but not with Gαs (*Right*) (IP_{GPR151} WT: 1 ± 0, KO: 0.03 ± 0.01, $n = 5$, unpaired *t* test, ***$P < 0.0001$; Input Gαo1/2 WT: 1 ± 0, KO: 0.98 ± 0.05, $n = 5$, unpaired *t* test, not significant (n.s.): $P = 0.84$; IP Gαo1/2 WT: 1 ± 0, KO: 0.31 ± 0.09, $n = 5$, unpaired *t* test, $P < 0.0001$). The double arrow indicates the double band corresponding to GPR151 WB signal. Arrowheads indicate Gαo1 and Gαs WB signals. (*D*) LANCE cAMP competition assay in CHO–K1 cells under forskolin stimulation (log Forskolin nM) shows higher cAMP levels in parental control cells (red) than in GPR151-expressing cells (green). Pertussis toxin (PT) decreases the EC_{50} ($n = 2$ technical triplicates per response curve, one-way ANOVA for EC_{50} values, Bonferroni's multiple-comparison test, ****$P < 0.0001$, CHO–K1–Control vs. CHO–K1–GPR151, $P > 0.99$, CHO–K1–Control vs. CHO–K1–Control+PTX, ***$P = 0.0004$, CHO–K1–GPR151 vs. CHO–K1–GPR151+PTX). (*E*) Knockdown of *Gpr151* in IPN after injection of lentivirus (LV)–shRNA–GFP in the MHb of WT mice in comparison with mice injected with LV–scramble. LP, lateral posterior nucleus of the thalamus; MD, medio dorsal nucleus of the thalamus; VPLp, ventral posterior lateral nucleus of the thalamus; Pul, pulvinar of the thalamus; CM, centromedian nucleus of the thalamus; sm, stria medularis; 3V, third ventricle; ZI, zona incerta; TH, thalamus; M, midbrain; Aq, cerebral aqueduct. Dashed lines F and G indicate the sectioning planes used for micrographs F and G. (Scale bar, 100 μm.) (*F*) *Gpr151*–KO and shRNA-injected mice have higher cAMP levels in the IPN than WT and LV–scramble control mice (KO vs. WT: $n = 15$, unpaired *t* test, **$P = 0.0016$, shRNA3 vs. scramble $n = 8–6$, unpaired *t* test, $P = 0.07$). Data are represented as mean ± SEM. See *SI Appendix*, Table S3 for details of statistical analysis.

as SV glycoprotein 2A (SV2A) and voltage-dependent anion channels (VDAC2) (23) and ATPases involved in regulating the functional dynamics of the presynapse (including the sodium/potassium ATPase composed of AT1A2 and AT1A3 (catalytic α-subunits), AT1B1 and AT1B2 (structural β-subunits), the calcium ATPase (AT2A2 and AT2B3), and the H+ transporting ATPase (AT5B) (24) (Fig. 2*B* and *SI Appendix*, Table S1 and Figs. S5–S7 of GO analysis). Association of GPR151 with these proteins in mass spectrometry is consistent with iEM localization at SVs. Besides SV proteins, we detected a strong interaction with the G-alpha inhibitory subunit *Gnao1* (protein name Gαo1), a heterotrimeric guanine nucleotide-binding G proteins involved in intracellular signal transduction (Fig. 2*B*). To confirm this interaction, we performed immunoprecipitations and Western blot analysis of IPN extracts from WT and KO mice. As shown in Fig. 2*C*, GPR151 associates with Gαo1 but not with the G-alpha stimulatory subunit (Gαs). TRAP data collected from MHbs of $ChAT^{DW176}$ TRAP mice show that Gαo1 is the most abundant inhibitory Gi/o subunit in cholinergic MHb neurons and is expressed at similar levels in WT and *Gpr151*–KO mice (Dataset S2 and *SI Appendix*, Table S2).

To further validate the interaction of GPR151 with Gαo1, which inhibits adenylyl cyclase activity and decreases intracellular cAMP, we generated a stable cell line expressing GPR151 with a SNAP-tag. We used CHO–K1 cells, which express high levels of Gαo1. GPR151 expression at the membrane was validated by SNAP and GPR151 immunostaining and Western blot (*SI Appendix*, Fig. S8 *A* and *B*). Next, we measured cAMP levels upon forskolin stimulation using the LANCE cAMP competition assay. The half maximal effective concentration (EC_{50}) of forskolin of GPR151-expressing CHO–K1 cells was significantly higher than their parental cells CHO–K1 (Fig. 2*D*), suggesting that GPR151 is constitutively active and decreases cAMP, buffering the stimulatory effect of forskolin. Next, we treated the cells with pertussis toxin (PT), which inactivates Gαi/o proteins (25). PT had a strong effect on cAMP production stimulated by forskolin in GPR151-expressing CHO–K1 cells (Fig. 2*D*), indicating that PT blocks a large portion of the inhibitory response mediated by Gαo1. Together these results provide evidence that GPR151 is constitutively active and couples to Gαo1 to decreases cAMP levels. The constitutive activity of GPR151 is not unexpected, since it lacks the DRY motif, which plays an essential role in the interaction with G proteins in class A GPCRs (26).

Given that GPR151 coimmunoprecipitates with Gαo1 in mouse brain extracts and decreases cAMP levels in CHO–K1 cells, we wanted to evaluate whether cAMP levels are different in KO mice. We conducted cAMP ELISAs of IPN samples of WT and *Gpr151*–KO mice. We observed that cAMP levels are higher in *Gpr151*–KO IPN homogenates than in WT mice (Fig. 2*F*). Next, we screened for a short hairpin RNA (shRNA) against *Gpr151* that showed suitable down-regulation of *Gpr151* in vitro (*SI Appendix*, Fig. S9 *A* and *B*) and in vivo (Fig. 2*E* and *SI Appendix*, Fig. S9*C*). WT mice injected into the MHb with the shRNA against *Gpr151* showed a strong trend of increased cAMP levels ($P = 0.07$) relative to mice injected with a scrambled shRNA (Fig. 2*F*). These results suggest that GPR151 interacts with the Gαo1 inhibitory subunit to reduce cAMP at habenular synapses in the IPN.

GPR151 Contributes to Synaptic Plasticity. The localization of GPR151 at the presynaptic membrane and SVs, and its association with presynaptic proteins known to regulate the dynamics of neurotransmitter release, suggested that GPR151 could modulate the synaptic activity of habenular terminals. To explore this possibility, we first recorded spontaneous glutamatergic miniature excitatory postsynaptic currents (mEPSCs) in IPN neurons. We observed that the frequency, but not the amplitudes, of mEPSCs is increased in *Gpr151*–KO mice (Fig. 3 *A*–*C*), indicating that GPR151 acts presynaptically and influences the release probability of SVs at basal conditions. In the absence of a known ligand to activate GPR151, we employed optogenetics to evaluate whether light-evoked currents would differ between WT and *Gpr151*–KO mice crossed to *Chat*–ChR2 mice (11) expressing channelrhodopsin-2 in cholinergic neurons (Fig. 3*D*). We used these mice since the majority of GPR151-expressing neurons (70%) are cholinergic neurons (*SI Appendix*, Fig. S2 *A* and *B*). Glutamatergic evoked eEPSCs were elicited by brief (5 ms) blue light pulses (Fig. 3*E*). The amplitude of light eEPSCs was significantly smaller in *Chat*–ChR2x*Gpr151*–KO than in *Chat*–ChR2 mice (Fig. 3 *E* and *F*), and this was partially rescued in *Chat*–ChR2x*Gpr151*–KO mice injected with a rescue virus (AAV2/1–*Gpr151*) expressing *Gpr151* specifically in MHb (*SI Appendix*, Fig. S10*A*). Addition of forskolin, which raises cAMP levels, increased the amplitude of light eEPSCs in *Chat*–ChR2 mice (from 978 ± 129 pA to 1615 ± 155 pA, unpaired *t* test, $^*P = 0.01$) (Fig. 3 *F* and *G*). However, the amplitude was not altered in *Chat*–ChR2x*Gpr151*–KO upon forskolin application and remained smaller than WT levels (from 479 ± 62 pA to 390 ± 153 pA) (Fig. 3 *F* and *G*). This suggests that the absence of GPR151 compromises the coupling of cAMP signaling to neurotransmitter release machinery in habenula neurons.

Next, we used the Paired Pulse Ratio (PPR) to measure presynaptic release probability upon light stimulation. This stimulation paradigm measurement is commonly used to evaluate the effects of nicotine, which acts presynaptically to increase release probability at several synapses (27). At basal conditions, the PPR was similar between genotypes (compare black to red in Fig. 3 *H*–*J*). However, nicotine application in *Chat*–ChR2 slices increases the probability of the initial presynaptic release of the readily releasable pool of vesicles and therefore reduces the PPR (Fig. 3 *H* and *J*). In contrast, the PPR of *Chat*–ChR2x*Gpr151*–KO does not change upon nicotine application (Fig. 3 *I* and *J*). The increased rate of spontaneous release, decreased evoked EPSC, and unchanged PPR upon nicotine administration in *Gpr151*–KO mice point to a critical role of GPR151 in synaptic activity of habenular neurons.

***Gpr151*–KO Mice Show Reduced Sensitivity to Nicotine and Increased Self-Administration of High Nicotine Doses.** To understand the contribution of GPR151 to regulating the motivational properties of nicotine, we investigated its role in behaviors affected by nicotine. At baseline, *Gpr151*–KO mice showed no differences in anxiety-like behaviors measured by the elevated plus maze and in sensorimotor gating analyzed by the prepulse inhibition test, suggesting that GPR151 does not regulate basal affective-related behaviors (*SI Appendix*, Fig. S11 *A*–*C*). We assayed locomotor activity after an acute nicotine challenge, which reflects the sensitivity of an individual to nicotine (28). Baseline activity of *Gpr151*–KO mice at minute 0 was similar to WT (Fig. 4*A*). However, acute nicotine-induced hypolocomotion was significantly less prominent in *Gpr151*–KO mice (Fig. 4*A*), indicating that *Gpr151*–KO mice have reduced sensitivity to the motor-depressing property of nicotine. To measure nicotine tolerance, we performed daily acute injections of nicotine. WT mice showed a decreased effect of nicotine on locomotion over consecutive days, but *Gpr151*–KO mice did not demonstrate an adaptive response to repeated injection of nicotine (*SI Appendix*, Fig. S11*D*).

To rule out a developmental effect of GPR151 in habenular function, we injected adult *Gpr151*–KO mice with a rescue virus for reexpression of *Gpr151* and WT adult mice with virus expressing an shRNA against *Gpr151*. Viruses were injected bilaterally into the MHb, and presence or absence of GPR151 expression in the habenula, along the FR and at the IPN, was validated in the injected mice by immunohistochemistry (Fig. 2*E* and *SI Appendix*, Figs. S9*C* and S10*B*). WT mice displayed nicotine-induced hypolocomotion at all nicotine doses in a dose-dependent

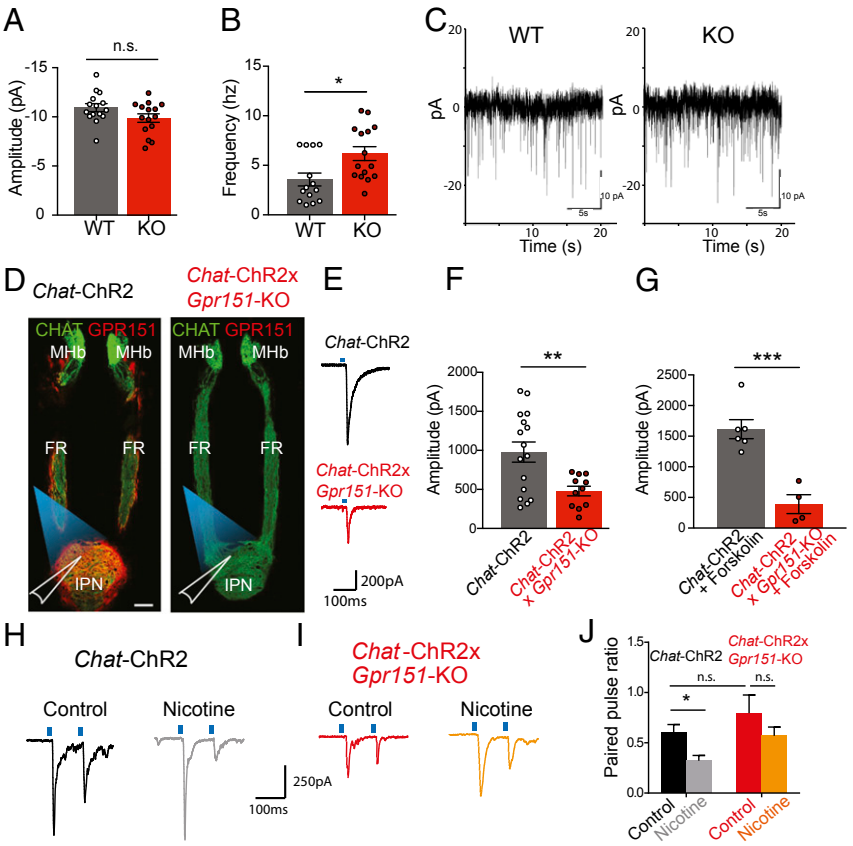

Fig. 3. GPR151 contributes to synaptic plasticity. (*A*) Average amplitude of spontaneous miniature mEPSCs in postsynaptic IPN neurons recorded during 20 s was not different between WT and *Gpr151*–KO mice ($n = 15$; unpaired t test, not significant [n.s.]: $P = 0.08$). (*B*) Average frequency rates of mEPSCs were significantly different between WT and *Gpr151–KO* mice ($n = 14$–15; unpaired t test, $^*P = 0.01$).(*C*) Example traces of mEPSCs of WT and *Gpr151*–KO mice. (*D*) Chat–ChR2–EYFP mice were crossed to *Gpr151*–KO for optogenetic recordings. Angled brain sections showing ChR2 (green) and GPR151 (red) in MHb–FR–IPN axis in Chat–ChR2 and loss of GPR151 signal in Chat–ChR2xGpr151–KO. Chat–ChR2 terminals in the IPN were optogenetically stimulated, and postsynaptic IPR neurons were recorded. (Scale bar, 100 μm.) (*E* and *F*) Amplitude of the first blue light evoked EPSC is reduced in *Chat*–ChR2x*Gpr151*–KO mice (red) compared to *Chat*–ChR2 mice (gray) ($n = 16$–11, unpaired t test, $^{**}P = 0.0056$). (*G*) Forskolin increases the previously observed difference of the amplitude of light evoked EPSCs in *Chat*–ChR2 neurons, compared to *Chat*–ChR2x*Gpr151*–KO neurons ($n = 6$–4, unpaired t test, $^{***}P = 0.0007$). (*H* and *I*) Example traces of paired-pulse ratio (PPR) recordings after vehicle or nicotine. (*J*) Nicotine-induced decreases in PPR were absent in *Chat*–ChR2x*Gpr151*–KO mice ($n = 17$ WT control, 8 WT nicotine, 8 KO control, 10 KO nicotine, Kruskall–Wallis test, Dunn's multiple comparisons test, $^*P < 0.05$). Data are represented as mean ± SEM. See *SI Appendix*, Table S3 for details of statistical analysis.

manner, while *Gpr151*–KO mice did not show a further decrease of locomotion at the higher doses (Fig. 4*B*). The absence of nicotine-induced hypolocomotor effects observed in *Gpr151*–KO mice was recapitulated in shRNA-injected mice, while reexpression of *Gpr151* in *Gpr151*–KO mice restored sensitivity to nicotine-induced hypolocomotion (Fig. 4*B*). These results show that *Gpr151*–KO mice are less sensitive to high doses of nicotine and do not show behavioral plasticity in response to repeated exposures of nicotine.

To determine whether GPR151 regulates the reinforcing properties of nicotine, we examined WT and *Gpr151*–KO mice in a self-administration task. First, mice underwent training to respond for food rewards in operant chambers where presses on the active lever resulted in the delivery of food pellets under a fixed-ratio 5 time-out 20 s (FR5TO20) schedule of reinforcement. No differences were observed in the acquisition of lever-pressing behavior (*SI Appendix*, Fig. S11 *E* and *F*). We determined if nicotine (1 mg/kg, s.c.) can reduce responding for food rewards in this task in WT and *Gpr151*–KO mice. In saline treated mice, the number of food pellets earned by WT mice (9.9 ± 0.8) and *Gpr151*–KO mice (11.8 ± 0.5) was comparable (Fig. 4*C*). Upon nicotine administration, WT mice responded significantly less to food rewards than saline WT controls, consistent with the anorectic effect of nicotine on food intake. However, this anorectic response was much less pronounced in *Gpr151*–KO mice (Fig. 4*C*) reflecting a reduced sensitivity to nicotine-induced suppression of appetite. Using the same paradigm but pairing the lever pressing to intravenous (i.v.) infusion of nicotine, we investigated the role of GPR151 in nicotine reinforcement. As expected, WT mice responded for self-administered nicotine infusions according to a known inverted U-shaped dose–response curve (19) (Fig. 4*D*). Notably, *Gpr151*–KO mice self-administered far more nicotine at a high nicotine dose than WT littermate mice (Fig. 4*E*). This pattern of responding to nicotine, particularly at higher unit doses of the drug, is similar to that previously reported in α5 nAChR subunit KO mice and in rats in which α5 subunits are selectively knocked down in Hb–IPN (19), suggesting reduced sensitivity to the aversive effects of high doses of nicotine. Reexpression of GPR151 in the MHb of *Gpr151*–KO mice reduced self-administration of the 0.4 mg/kg nicotine dose to levels similar to WT mice (Fig. 4 *F* and *G*). Consistent with the locomotor behavioral tests (Fig. 4 *A* and *B*), both the reduction in the anorectic effects of nicotine and the fact that *Gpr151*–KO mice self-administer more nicotine at high doses suggest that the KO mice are resistant to the aversive and malaise-inducing effects of nicotine. Taken together,

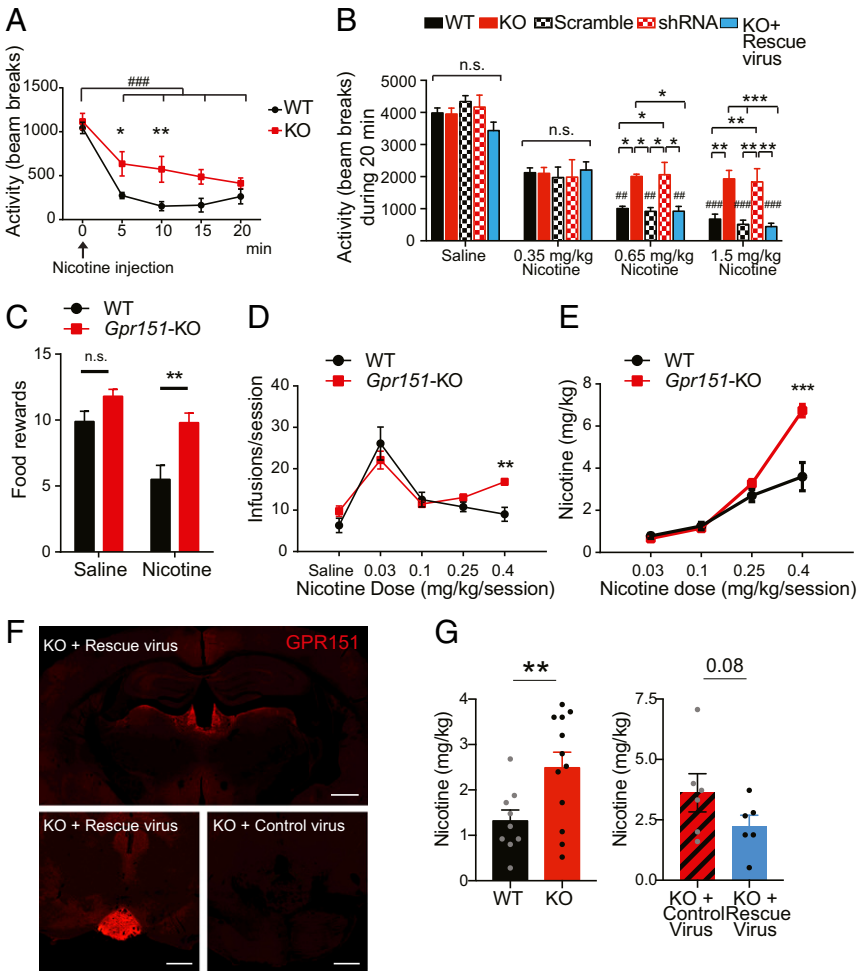

Fig. 4. *Gpr151*–KO mice show reduced sensitivity to nicotine and self-administer more nicotine at a high dose. (*A*) Nicotine-induced hypolocomotion (0.65 mg/kg, i.p.) is significantly diminished in *Gpr151*–KO mice ($n = 7$ per genotype; repeated-measures (RM) two-way ANOVA, Bonferroni multiple comparisons $^{*}P < 0.05$, $^{**}P < 0.01$ for genotype; Tukey's multiple comparisons test, $^{\#\#\#}P < 0.001$ for time in both groups). (*B*) Hypolocomotion is observed at the higher 2 doses of nicotine (0.65 and 1.5 mg/kg) in WT mice, WT mice injected with AAV2.1–scramble–shRNA (scramble) and in *Gpr151*–KO mice injected with AAV2.1–CAG–*Gpr151* (rescue) in the MHb, but not in *Gpr151*–KO mice and in WT mice injected with AAV2.1–shRNA against *Gpr151* (shRNA) in the MHb. ($n = 7$–8 per genotype, RM two-way ANOVA, Tukey's multiple comparison test, $^{*}P < 0.05$, $^{**}P < 0.01$, $^{***}P < 0.001$ for genotype; $^{\#\#}P < 0.01$, $^{\#\#\#}P < 0.001$ compared to 0.35 mg/kg nicotine within the same genotype). (*C*) Average number of food rewards after injection of saline or nicotine (1 mg/kg, s.c.). *Gpr151*–KO mice are resistant to the anorectic effect of nicotine ($n = 10$ per group, RM two-way ANOVA, Bonferroni's multiple comparisons test, $^{**}P < 0.01$ compared to WT). (*D*) *Gpr151*–KO mice earned significantly more nicotine infusions at the higher nicotine dose (0.4 mg/kg) ($n = 4$–8, RM two-way ANOVA, Bonferroni's multiple comparisons test, $^{**}P < 0.01$ compared to WT). (*E*) Total amount of nicotine self-administered at each dose ($n = 4$–8, RM two-way ANOVA, Bonferroni's multiple comparisons test, $^{***}P < 0.001$ compared to WT). *Gpr151*–KO mice self-administer a significantly higher amount of nicotine at the highest 0.4 mg/kg/session dose. (*F*) Reexpression of GPR151 in the MHb and IPN terminals of *Gpr151*–KO mice injected with AAV2.1–*Gpr151* visualized by GPR151 immunoreactivity and comparison with *Gpr151*–KO mice injected with AAV2/1–EGFP control virus. (Scale bar, 500 μm.) (*G*) At the highest nicotine dose (0.4 mg/kg/session), *Gpr151*–KO mice injected with AAV2.1–*Gpr151* rescue virus self-administered less nicotine (*Left*) to similar levels as WT (*Right*) ($n = 6$–12, unpaired *t* test, $^{**}P < 0.01$). Data are represented as mean ± SEM. See *SI Appendix*, Table S3 for details of statistical analysis. n.s., not significant.

these results demonstrate that GPR151 is critical for the inhibitory control exerted by the MHb in limiting drug and food intake.

Discussion

The emerging role of the habenula in processing reward-related and aversive signals has led to investigation of this brain circuit for identification of modulatory mechanisms that may provide common avenues for the development of new approaches toward the treatment of addiction. In this study, we demonstrate that the orphan receptor GPR151 regulates habenular neuron synaptic function and modulates nicotine intake. We find that GPR151 is selectively enriched in habenular presynaptic structures where it regulates synaptic transmission. This is similar to the roles of other GPCRs, including dopamine D2 and cannabinoid and opioid receptors, which have been localized at other presynaptic termini and shown to inhibit evoked synaptic transmission (29). GPCRs at the AZ regulate fast transmission by local action of the dissociated G beta–gamma complex (Gβγ) on exocytosis, while GPCRs distant from the AZ modulate neurotransmission through second-messenger cascades (29). GPR151 is both at the AZ and at the perisynapse where it couples to the G-inhibitory αo1 subunit to decrease cAMP and regulate synaptic release. Gαo1 and Gβ1 subunits have been localized in SVs and DCVs in neurons (23, 30), suggesting the presence of preassembled GPR151/G protein-signaling complexes in vesicles that can be transported to the plasma membrane upon neuronal stimulation. Interestingly, GPR151 can be activated by acidic conditions in vitro (31). Acidification also occurs after neuronal injury and induces pain and hyperalgesia. *Gpr151* messenger RNA (mRNA) has been shown to increase during neuropathic pain induced by

nerve ligation (32, 33), suggesting that further studies will be required to examine its role in pain.

The present studies suggest that enhanced cAMP levels in habenular terminals of *Gpr151*–KO mice are responsible for the behavioral changes observed with nicotine. cAMP facilitates neurotransmission by increasing release probability at central excitatory synapses (34). Depletion of presynaptic cAMP levels also suppresses neurotransmission in habenular neurons (35). Increases in cAMP signaling are a common adaptation following chronic morphine treatment (36), and activation of CB1R also modifies synaptic efficacy (37). Phosphorylation by cAMP-dependent kinases regulates the rate of desensitization of nAChRs (38), and specific PKA phosphorylation sites are modulated differently by acute or chronic exposure to nicotine (36, 37). It has also been shown that deficits in cAMP signaling can alter nicotine intake in mice (39). Given our demonstration that loss of *Gpr151* alters the frequency of spontaneous mEPSCs without altering their amplitude, and that it is present on SVs carrying SV2A and other core proteins, it is probable that GPR151 can act directly on the core complex to regulate vesicle release. This is consistent with studies showing that altering the functions of synaptotagmin (40), SNAP-25, SV2A (41), and of other proteins of the core synaptic protein complex involved in docking and fusion leads to a phenotype of decreased evoked EPSC amplitude and increased mEPSC frequency. The role of GPR151 in the modulation of cAMP levels suggests also that its function in MHb neurons may include cAMP-mediated phosphorylation of nAChRs or other proteins present in MHb terminals. For example, the demonstration that the sodium/potassium pump ATP1A3/B1 is present in the immunoprecipitates of GPR151, and its demonstrated role in control the readily releasable pool size at glutamatergic synapses (42), suggests this as an additional possible target of GPR151 regulation.

Given the modulatory role of GPR151 on the response to nicotine that we have demonstrated here, it is of interest to understand its role in other behaviors modulated by the MHb (43). Interestingly, UK biobank studies have recently shown that GPR151 loss-of-function alleles are associated with lower body mass index and protection from diabetes type 2 (44). Related to this, we have recently found that nicotine acts on MHb neurons, which are polysynaptically connected to the pancreas, to stimulate increases in blood glucose levels, and prolonged exposure to this action of nicotine can precipitate the emergence of diabetes in laboratory rodents (39). This suggests that GPR151 may influence diabetes vulnerability, particularly in smokers, by regulating MHb function.

Finally, our studies suggest GPR151 as a candidate target for therapies preventing drug abuse because: it is exclusively localized in axonal projections of habenular neurons, decreasing the likelihood of developing side effects due to alterations in other brain circuits or in the peripheral nervous system; it modulates neurotransmission and affects sensitivity to nicotine; habenular synapses also contain high levels of opioid and cannabinoid receptors; and it belongs to the highly druggable class A family of GPCRs that can be screened with cAMP assays. We hope our work stimulates additional interest in GPR151, as we believe an agonist to this receptor could be a valuable therapeutic in efforts to reduce the adverse impacts of drug abuse on public health.

Materials and Methods

Animals. All procedures involving mice were approved by The Rockefeller University and Mount Sinai Institutional Animal Care and Use Committee and were in accordance with the NIH guidelines (45). See *SI Appendix, Supplementary Experimental Procedures* for details.

Coimmunoprecipitations, Western Blot, and Proteomic Analysis. Coimmunoprecipitations for mass spectrometry analysis were performed using M-270 Epoxy Dynabeads (Invitrogen) with three different GPR151 antibodies. Coimmunoprecipitations for Western blot analysis were done using Dynabeads Protein G (Invitrogen) coupled to GPR151 antibodies. See *SI Appendix, Supplementary Experimental Procedures* for further details.

Immunohistochemistry of Human and Mouse Brain Samples and Quantification Analysis. Human brain tissues were obtained from the National Institute of Child Health and Human Development (NICHD) Brain and Tissue Bank from five donors, ranging between 22 and 52 y of age. Immunohistochemistry was performed in adult mice (8–12 wk) as described in ref. 22. See *SI Appendix, Supplementary Experimental Procedures*.

Electron Microscopy. Preembedding and postembedding nanogold labeling was performed as in ref. 12. See *SI Appendix, Supplementary Experimental Procedures*.

TRAP and RNA Sequencing (RNA-Seq). Three biological replicates were used for TRAP analysis. Each replicate contained the habenulae from five CHAT–EGFP–L10a transgenic mice (males and females 8–12 wk old). See *SI Appendix, Supplementary Experimental Procedures*.

Electrophysiological Recordings. IPN neurons were patch-clamped at −70 mV. Presynaptic MHb fibers were excited with a 473-nm blue light laser stimulation and a pulse length of 5 ms. See *SI Appendix, Supplementary Experimental Procedures*.

Behavioral Analysis. All behavioral studies were conducted blind to the genotype of the tested mice, and only male mice 8–16 wk old were used. See *SI Appendix, Supplementary Experimental Procedures*.

I.v. Nicotine Self-Administration Procedure. Mice were mildly food restricted to 85–90% of their free-feeding body weight and trained to press one of two levers in an operant chamber (Med-Associates, Inc.) for food pellets under a FR5TO20 reinforcement schedule. Mice underwent jugular catheter implantation, and once stable responding was reestablished, subjects were permitted to respond for i.v. nicotine infusions during 1 h daily sessions, 7 d per week, 3–5 d for each dose of nicotine in ascending order, with saline last. See *SI Appendix, Supplementary Experimental Procedures* for details.

Statistical Analysis. See *SI Appendix*, Table S3 for details of statistical analysis. Results are presented as means ± SEM.

Data Availability. The authors declare that all data supporting the findings of this study are available within the paper and *SI Appendix*. The GEO accession number for the RNA-Seq data is GSE143854.

ACKNOWLEDGMENTS. We thank Kunihiro Uryu, Nadine Soplop, Milica Tešić, Juncheng Li, Rada Norinski, Awni Mousa, and Laura Kus for technical assistance. Human tissue was obtained from the NICHD Brain and Tissue Bank, University of Maryland, Baltimore, MD. H.M. was supported by the Leona M. and Harry B. Helmsley Charitable Trust and Sohn Conferences Foundation. This work was also supported by the Leon Black Family Foundation (I.I.-T. and N.H.), National Institute on Drug Abuse (NIDA) (1P30 DA035756-01) (I.I.-T.,N.H.), DA020686 (P.J.K.), NIDA UG3 DA048385 (P.J.K. and I.I.-T.), and Howard Hughes Medical Institute (N.H.).

1. WHO, Tobacco. https://www.who.int/news-room/fact-sheets/detail/tobacco. Accessed 24 June 2019.
2. Office of the Surgeon General, Surgeon General releases advisory on E-cigarette epidemic among youth. https://www.hhs.gov/about/news/2018/12/18/surgeon-general-releases-advisory-e-cigarette-epidemic-among-youth.html. Accessed 24 August 2019.
3. G. F. Koob, N. D. Volkow, Neurobiology of addiction: A neurocircuitry analysis. *Lancet Psychiatry* **3**, 760–773 (2016).
4. D. J. Nutt, A. Lingford-Hughes, D. Erritzoe, P. R. Stokes, The dopamine theory of addiction: 40 years of highs and lows. *Nat. Rev. Neurosci.* **16**, 305–312 (2015).
5. S. Lammel, B. K. Lim, R. C. Malenka, Reward and aversion in a heterogeneous midbrain dopamine system. *Neuropharmacology* 76, 351–359 (2014).
6. B. Antolin-Fontes, J. L. Ables, A. Görlich, I. Ibañez-Tallon, The habenulo-interpeduncular pathway in nicotine aversion and withdrawal. *Neuropharmacology* **96**, 213–222 (2015).
7. V. Mathis, P. J. Kenny, From controlled to compulsive drug-taking: The role of the habenula in addiction. *Neurosci. Biobehav. Rev.* **106**, 102–111 (2019).
8. S. Molas, S. R. DeGroot, R. Zhao-Shea, A. R. Tapper, Anxiety and nicotine dependence: Emerging role of the habenulo-interpeduncular axis. *Trends Pharmacol. Sci.* **38**, 169–180 (2017).
9. H. Aizawa, M. Kobayashi, S. Tanaka, T. Fukai, H. Okamoto, Molecular characterization of the subnuclei in rat habenula. *J. Comp. Neurol.* **520**, 4051–4066 (2012).
10. S. Frahm *et al.*, An essential role of acetylcholine-glutamate synergy at habenular synapses in nicotine dependence. *eLife* **4**, e11396 (2015).

11. J. Ren *et al*., Habenula "cholinergic" neurons co-release glutamate and acetylcholine and activate postsynaptic neurons via distinct transmission modes. *Neuron* **69**, 445–452 (2011).
12. P. Y. Shih *et al*., Differential expression and function of nicotinic acetylcholine receptors in subdivisions of medial habenula. *J. Neurosci.* **34**, 9789–9802 (2014).
13. A. Görlich *et al*., Reexposure to nicotine during withdrawal increases the pacemaking activity of cholinergic habenular neurons. *Proc. Natl. Acad. Sci. U.S.A.* **110**, 17077–17082 (2013).
14. J. L. Ables *et al*., Retrograde inhibition by a specific subset of interpeduncular α5 nicotinic neurons regulates nicotine preference. *Proc. Natl. Acad. Sci. U.S.A.* **114**, 13012–13017 (2017).
15. J. P. Changeux, Nicotine addiction and nicotinic receptors: Lessons from genetically modified mice. *Nat. Rev. Neurosci.* **11**, 389–401 (2010).
16. T. E. Thorgeirsson *et al*., A variant associated with nicotine dependence, lung cancer and peripheral arterial disease. *Nature* **452**, 638–642 (2008).
17. C. D. Fowler, Q. Lu, P. M. Johnson, M. J. Marks, P. J. Kenny, Habenular α5 nicotinic receptor subunit signalling controls nicotine intake. *Nature* **471**, 597–601 (2011).
18. S. Frahm *et al*., Aversion to nicotine is regulated by the balanced activity of β4 and α5 nicotinic receptor subunits in the medial habenula. *Neuron* **70**, 522–535 (2011).
19. R. Salas, R. Sturm, J. Boulter, M. De Biasi, Nicotinic receptors in the habenulo-interpeduncular system are necessary for nicotine withdrawal in mice. *J. Neurosci.* **29**, 3014–3018 (2009).
20. J. Broms, B. Antolin-Fontes, A. Tingström, I. Ibañez-Tallon, Conserved expression of the GPR151 receptor in habenular axonal projections of vertebrates. *J. Comp. Neurol.* **523**, 359–380 (2015).
21. Y. Kobayashi *et al*., Genetic dissection of medial habenula-interpeduncular nucleus pathway function in mice. *Front. Behav. Neurosci.* **7**, 17 (2013).
22. S. Passlick, E. R. Thapaliya, Z. Chen, M. T. Richers, G. C. R. Ellis-Davies, Optical probing of acetylcholine receptors on neurons in the medial habenula with a novel caged nicotine drug analogue. *J. Physiol.* **596**, 5307–5318 (2018).
23. S. Takamori *et al*., Molecular anatomy of a trafficking organelle. *Cell* **127**, 831–846 (2006).
24. A. Taruno, H. Ohmori, H. Kuba, Inhibition of presynaptic Na(+)/K(+)-ATPase reduces readily releasable pool size at the avian end-bulb of Held synapse. *Neurosci. Res.* **72**, 117–128 (2012).
25. H. K. Fong, K. K. Yoshimoto, P. Eversole-Cire, M. I. Simon, Identification of a GTP-binding protein alpha subunit that lacks an apparent ADP-ribosylation site for pertussis toxin. *Proc. Natl. Acad. Sci. U.S.A.* **85**, 3066–3070 (1988).
26. J. Wess, Molecular basis of receptor/G-protein-coupling selectivity. *Pharmacol. Ther.* **80**, 231–264 (1998).
27. S. L. Wolfman *et al*., Nicotine aversion is mediated by GABAergic interpeduncular nucleus inputs to laterodorsal tegmentum. *Nat. Commun.* **9**, 2710 (2018).
28. P. B. Clarke, R. Kumar, The effects of nicotine on locomotor activity in non-tolerant and tolerant rats. *Br. J. Pharmacol.* **78**, 329–337 (1983).
29. K. M. Betke, C. A. Wells, H. E. Hamm, GPCR mediated regulation of synaptic transmission. *Prog. Neurobiol.* **96**, 304–321 (2012).
30. G. Ahnert-Hilger *et al*., Detection of G-protein heterotrimers on large dense core and small synaptic vesicles of neuroendocrine and neuronal cells. *Eur. J. Cell Biol.* **65**, 26–38 (1994).
31. M. Mashiko, A. Kurosawa, Y. Tani, T. Tsuji, S. Takeda, GPR31 and GPR151 are activated under acidic conditions. *J. Biochem*, mvz042 (2019).
32. F. E. Holmes *et al*., Targeted disruption of the orphan receptor Gpr151 does not alter pain-related behaviour despite a strong induction in dorsal root ganglion expression in a model of neuropathic pain. *Mol. Cell. Neurosci.* **78**, 35–40 (2017).
33. B. C. Jiang *et al*., Demethylation of G-protein-coupled receptor 151 promoter facilitates the binding of Krüppel-like factor 5 and enhances neuropathic pain after nerve injury in mice. *J. Neurosci.* **38**, 10535–10551 (2018).
34. T. Sakaba, E. Neher, Preferential potentiation of fast-releasing synaptic vesicles by cAMP at the calyx of Held. *Proc. Natl. Acad. Sci. U.S.A.* **98**, 331–336 (2001).
35. F. Hu, J. Ren, J. E. Zhang, W. Zhong, M. Luo, Natriuretic peptides block synaptic transmission by activating phosphodiesterase 2A and reducing presynaptic PKA activity. *Proc. Natl. Acad. Sci. U.S.A.* **109**, 17681–17686 (2012).
36. B. Bie, Y. Peng, Y. Zhang, Z. Z. Pan, cAMP-mediated mechanisms for pain sensitization during opioid withdrawal. *J. Neurosci.* **25**, 3824–3832 (2005).
37. I. Katona, T. F. Freund, Endocannabinoid signaling as a synaptic circuit breaker in neurological disease. *Nat. Med.* **14**, 923–930 (2008).
38. R. L. Huganir, A. H. Delcour, P. Greengard, G. P. Hess, Phosphorylation of the nicotinic acetylcholine receptor regulates its rate of desensitization. *Nature* **321**, 774–776 (1986).
39. A. Duncan *et al*., Habenular TCF7L2 links nicotine addiction to diabetes. *Nature* **574**, 372–377 (2019).
40. J. T. Littleton, M. Stern, K. Schulze, M. Perin, H. J. Bellen, Mutational analysis of Drosophila synaptotagmin demonstrates its essential role in Ca(2+)-activated neurotransmitter release. *Cell* **74**, 1125–1134 (1993).
41. K. L. Custer, N. S. Austin, J. M. Sullivan, S. M. Bajjalieh, Synaptic vesicle protein 2 enhances release probability at quiescent synapses. *J. Neurosci.* **26**, 1303–1313 (2006).
42. H. Poulsen *et al*., Phosphorylation of the Na+,K+-ATPase and the H+,K+-ATPase. *FEBS Lett.* **584**, 2589–2595 (2010).
43. P. J. Kenny, Common cellular and molecular mechanisms in obesity and drug addiction. *Nat. Rev. Neurosci.* **12**, 638–651 (2011).
44. C. A. Emdin *et al*., Analysis of predicted loss-of-function variants in UK Biobank identifies variants protective for disease. *Nat. Commun.* **9**, 1613 (2018).
45. National Research Council, *Guide for the Care and Use of Laboratory Animals* (National Academies Press, Washington, DC, ed. 8, 2011).
46. Allen Institute, Data from "Gpr151 - RP_060220_04_A08 - coronal." Allen Brain Atlas. http://mouse.brain-map.org/experiment/show/74724649. Accessed 13 February 2020.